
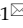



Review

# Sensing Using Rare-Earth-Doped Upconversion Nanoparticles

Shuwei Hao<sup>1</sup>, Guanying Chen<sup>1,2</sup>, Chunhui Yang<sup>1</sup>

1. School of Chemical Engineering and Technology, Harbin Institute of Technology, 150001 Harbin, People's Republic of China.
2. Institute for Lasers, Photonics and Biophotonics, Department of Chemistry, University at Buffalo, The State University of New York, Buffalo, New York, 14260, USA.

 Corresponding author: guanying@buffalo.edu, yangchh@hit.edu.cn.

© Ivyspring International Publisher. This is an open-access article distributed under the terms of the Creative Commons License (<http://creativecommons.org/licenses/by-nc-nd/3.0/>). Reproduction is permitted for personal, noncommercial use, provided that the article is in whole, unmodified, and properly cited.

Received: 2012.09.27; Accepted: 2012.12.06; Published: 2013.03.26

## Abstract

Optical sensing plays an important role in theranostics due to its capability to detect hint biochemical entities or molecular targets as well as to precisely monitor specific fundamental psychological processes. Rare-earth (RE) doped upconversion nanoparticles (UCNPs) are promising for these endeavors due to their unique frequency converting capability; they emit efficient and sharp visible or ultraviolet (UV) luminescence via use of ladder-like energy levels of RE ions when excited at near infrared (NIR) light that are silent to tissues. These features allow not only a high penetration depth in biological tissues but also a high detection sensitivity. Indeed, the energy transfer between UCNPs and biomolecular or chemical indicators provide opportunities for high-sensitive bio- and chemical-sensing. A temperature-sensitive change of the intensity ratio between two close UC bands promises them for use in temperature mapping of a single living cell. In this work, we review recent investigations on using UCNPs for the detection of biomolecules (avidin, ATP, etc.), ions (cyanide, mercury, etc.), small gas molecules (oxygen, carbon dioxide, ammonia, etc.), as well as for *in vitro* temperature sensing. We also briefly summarize chemical methods in synthesizing UCNPs of high efficiency that are important for the detection limit.

Key words: Upconversion, Nanoparticles, Biosensing, Chemical Sensing, Temperature Sensing.

## Introduction

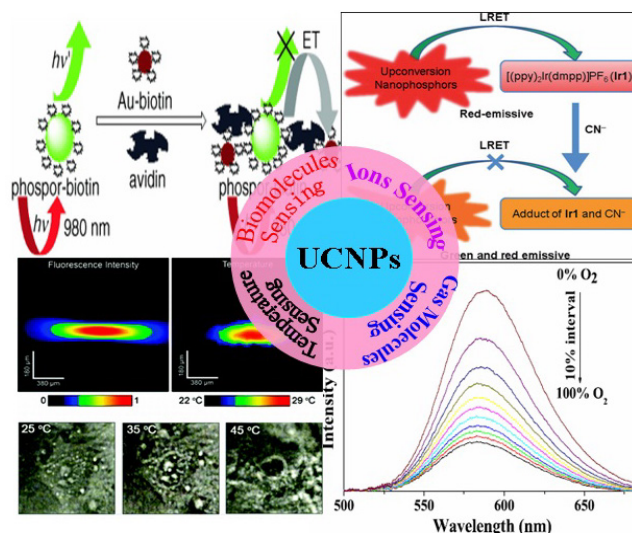
Rare earth (RE)-doped upconversion nanophosphors (UCNPs) can efficiently convert near-infrared (NIR) light into visible or ultraviolet (UV) luminescence using a stepwise multiphoton process in a system of real energy levels of RE ions which are embedded in an appropriate host lattice [1-4]. Along with the low cytotoxicity provided by the inorganic host lattice, this unique frequency converting capability imparts a number of advantages to UCNPs such as absence of autofluorescence, deep light penetration in tissues, and minimum photo-damage to living organisms [5,6]. These merits make them attractive in bioanalytical and biophysical studies. However, the low luminescent efficiency and the large size of UCNPs are two main limiting factors for

their biological applications. Smaller UCNPs with high luminescent efficiency has been being investigated in order to improve their performance in sensing applications as well as in other biophotonic and nanophotonic applications [7-11]. It has been shown that RE fluorides, in particular, RE<sub>3</sub> and AREF<sub>4</sub> (RE=rare earth; A = Li, Na, K) material, generally possess higher UC efficiency than the other UC host materials investigated (oxide, oxyfluoride, vanadates, oxysulfide, etc), due to their low phonon energies (< 400 cm<sup>-1</sup>) which minimized multiphonon-assisted nonradiative losses in the intermediate state and the emitting state of RE ions [12-14]. Hence, a range of chemical approaches have been being explored to fabricate high-quality small-sized RE-doped fluorides

nanocrystals (monodisperse, high uniform, well-shaped, phase-pure, and highly efficient) [15-19]. Among all synthetic techniques, thermal decomposition and hydro(solvo)thermal reaction are found to be two general strategies in producing fluoride nanophosphors [20-23]. Although the focus of this review is on the use of UCNPs in sensing applications, it will be helpful to briefly mention some recent results regarding high-quality and efficient UCNPs.

It is well known that bimolecular sensing is of great importance in biological detection and molecular medicine, while the real-time monitoring of the change of fundamental parameters, e.g., the pH value and the temperature in living cells, is important for understanding the programmed activities in cell. Molecular oxygen and carbon dioxide are involved in numerous biological and biochemical processes, and the harmful ammonia is released as a result of enzymatic activity [24-28]. The measurement of concentration of these gas molecules in biological fluid, therefore, is of particular importance for clinical medical diagnosis [25]. In addition, some hazardous ions, e.g., cyanide ions ( $\text{CN}^-$ ) and mercuric ions ( $\text{Hg}^{2+}$ ) are extremely toxic to mammals; selective detection and quantification of these poisonous ions in water, food or biological environment is necessary [29-31]. Although optical sensing techniques based on Stokes-shifted downconversion fluorophors (e.g., dyes, quantum dots) are engaged in these sensing applications, it is important to develop new sensing techniques that have higher sensitivity and more flexibility [32]. UCNPs utilize real intermediate energy states of RE ions and step-wise multi-photon processes to emit visible or UV luminescence when excited at low-energy NIR light of  $1-10^3 \text{ W/cm}^2$ , typically at  $\sim 980 \text{ nm}$  [33]. The efficiency of UC process is generally by orders of magnitude higher than the multiphoton absorption induced fluorescence where the virtual intermediate states and an excitation density of  $10^6 \text{ W/cm}^2$  provided by a femtosecond laser are utilized [33,34]. As the NIR excitation wavelength of  $980 \text{ nm}$  is transparent to tissues or biomolecules, non-invasive sensing detection in deep tissues is permitted [35-37]. Moreover, the emission wavelength of UCNPs has a large anti-Stokes shift when compared with the excitation line. The fluorescence of indicators induced by energy transfers from UCNPs can generally be isolated from the scattering excitation light and Stokes-shifted autofluorescence in tissues or biomolecules [38]. This unique feature results in a high signal to background ratio, allowing hint detections of interested entities. Here, we summarize recent works on the use of UCNPs in different sensing applications. It encompasses two sections of (i) synthesis of UCNPs, and (ii) sensing applications. Figure 1 il-

lustrates the scheme of the sensing section that includes bio-molecular sensing (e.g., avidin, ATP, etc), ions sensing (cyanide, mercury, etc), gas molecules sensing (oxygen, carbon dioxide, ammonia, etc), as well as temperature sensing in live cells.



**Figure 1.** An illustration of structured sensing topics in this work. Adapted from references [81, 89, 95, 113].

## 2. Synthesis of Rare Earth Doped Fluoride Nanomaterials

In the past decade, many efforts have been dedicated to prepare the RE-doped fluoride UCNPs with high quality in order to meet the requirement of various bio-related applications, in particular, smaller UCNPs with size compatible to biomolecules or protein. Up to date, the established preparation methods encompass thermal decomposition, hydro(solvo)thermal, ionic liquids-based synthesis, co-precipitation, combustion, and sol-gel. Among them, the thermal decomposition method and the hydro(solvo) thermal method are two general and important approaches for controlled synthesis of uniform fluoride NPs. Up to now, most of sensing applications are based on nanoparticles prepared using these two approaches. Hence, we will discuss their synthetic chemistry first in this section, and then discuss the use of them for sensing applications in section 3.

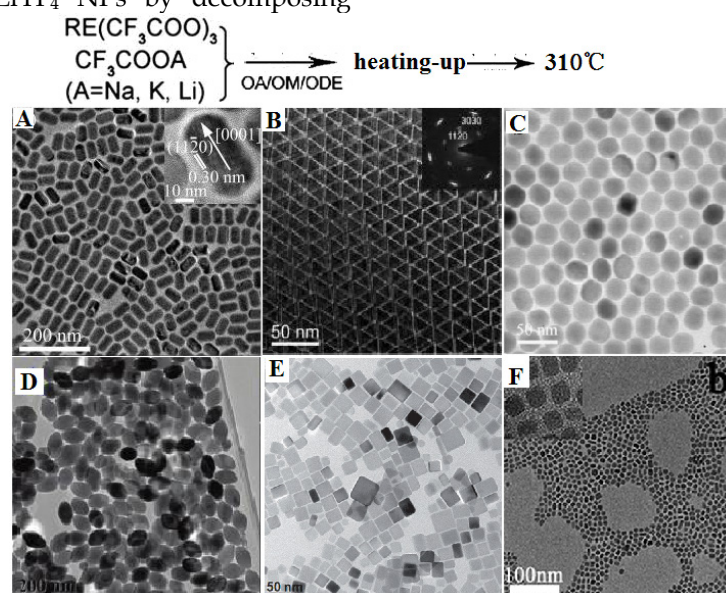
### 2.1 Thermal Decomposition Method

In a typical thermal decomposition procedure, organic precursors (lanthanide or alkali trifluoroacetate) are decomposed in a high-boiling organic solvent with the assistance of one or more surfactants, yielding corresponding metal fluorides at an elevated temperature [39-41]. A precise control over the nanocrystal phase, size and morphologies can be achieved by varying reaction parameters such as, the composi-

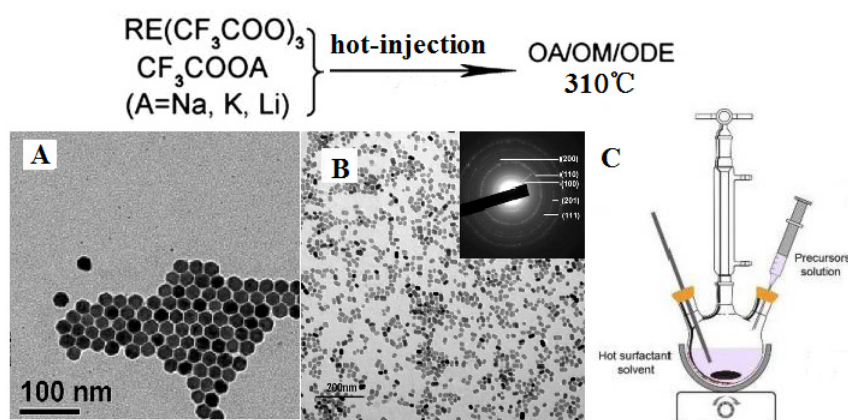
tion and amount of precursors, the amount of surfactants (e.g., OA and/or OM), solvent (e.g., ODE) as well as reaction temperature and time. In addition, the loading ways of precursors are also important of the final product, which encompass two types: (i) the “heating-up method”; (ii) the “hot-injection method” [42]. In the “heating-up” process, the temperature of reaction solution is elevated from room temperature to a specific high temperature to produce NPs, while the “hot-injection” process employ the way of the injection of pertinent precursors into a hot solution containing the high-boiling solvent and surfactants. Despite that the fundamental reaction chemistry are identical for these two different types of loading ways, the nucleation rate and the phase transition processes are quite different in these two methods.

Based on the principle described above, Yan *et al.* first reported the preparation of high-quality  $\text{NaYF}_4$  nanocrystals and monodispersed  $\text{LaF}_3$  triangular nanoplates (Figure 2A and B) through a heating-up process via decomposition of appropriate metal trifluoroacetate in the presence of oleic acid (OA)/1-octadecene (ODE) [43]. Subsequently, a wide range of high quality RE-doped fluoride NPs of various types are produced, which exhibit highly efficient UC emissions. Examples are as follows. (i) Zhang group reported the synthesis of monodispersed Yb,Er or Yb,Tm co-doped hexagonal  $\text{NaYF}_4$  nanocrystals with narrow size distribution by consuming a stoichiometric amount of lanthanide chlorate precursors at room temperature [44]. The uniformity of these nanoparticles is realized through the strong interaction between small cubic  $\text{NaYF}_4$  crystal nuclei or particles. (ii) Chen *et al.* prepared 80 nm sized monodispersed  $\text{LiYF}_4$  NPs by decomposing

lanthanide and adequate lithium trifluoroacetates at 330 °C in 30 mL oleic acid and 30 mL 1-octadecene solution [45]. The as-synthesized  $\text{LiYF}_4$  NPs displays high quantum yield  $\sim 1.2\%$ , which is almost 4 times higher than the highest UC luminescence quantum yield reported to date. A large amount of lithium precursors provide an efficient nucleation and grow rates, leading to form uniform products, while the tetragonal crystal of  $\text{LiYF}_4$  provide a unique crystal field for a high UC efficiency. (iii) Liu group synthesized  $\text{KMnF}_3$  nanoparticles by heating pre-prepared manganese oleate precursor and lanthanide chlorate precursors at 290 °C in a mixture solution of oleylamine (1 mL), oleic acid (1 mL), and 1-octadecene (8 mL) [46]. The prepared  $\text{KMnF}_3$  NPs can emit novel pure single-band UC emissions in the red and near-infrared spectral regions owing to an efficient energy transfer from the dopant  $\text{RE}^{3+}$  ions to the  $\text{Mn}^{2+}$  ions. (iv) More recently, Lin group heated the barium trifluoroacetate and lanthanide trifluoroacetate at 300 °C in a mixture solution of oleic acid (10 mL) and 1-octadecene (10 mL) and synthesized  $\text{BaGdF}_4$  nanocrystals with well-shaped (Figure 2F) [47]. It is clear from examples that, utilizing heat-up thermal decomposition method, a wide range of high-quality UC NPs including  $\text{NaYF}_4$  [48,49],  $\text{NaGdF}_4$  [50,51],  $\text{LiYF}_4$  [52],  $\text{NaYbF}_4$  [53],  $\text{Na}_3\text{ScF}_6$  [54],  $\text{YF}_3$  [55],  $\text{GdOF}$  [56], *etc.* can be synthesized. However, a judicious selection of reaction parameters is of particular importance in producing different types of fluoride nanoparticles. One challenge for “heating-up method” is that it is difficult to directly pare hexagonal  $\text{AREF}_4$  nanoparticles with size smaller than 100 nm; two or more steps have to be employed to realize this goal.



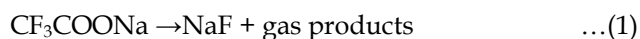
**Figure 2.** Representative shapes of various RE fluoride nanomaterials by heating-up process in thermal decomposition reaction. Reproduced with permission from references [43-47].



**Figure 3.** (A) RE-doped cubic  $\text{NaYF}_4$  nanoparticles [59], (B) RE-doped hexagonal  $\text{NaYF}_4$  nanoparticles [42], (C) the hot-injection reaction equipment to prepare nanoparticles in (A) and (B). Reproduced with permission from the corresponding references.

Figure 3 (A, B) shows two examples of RE-doped  $\text{NaYF}_4$  nanomaterials synthesized by a hot-injection method, while the setup of hot-injection equipment is displayed in Figure 3 (C). Shan *et al.* investigated the growth mechanism of  $\text{NaYF}_4$  nanocrystals and divided the synthesis reaction into two stages as follows [57]:

Stage I,  $a$ -UCNPs formation between 250 and 310  $^\circ\text{C}$ .



Stage II,  $\beta$ -UCNPs formation,  $\geq 310^\circ\text{C}$ :



Reaction 1 is a process in which sufficient NaF reactants is produced and then interact with RE trifluoroacetate to produce nucleation of  $\alpha$ - $\text{NaYF}_4$  in reaction 2 [58]. Capobianco *et al.* [59] prepared mono-dispersed Yb/Er and Yb/Tm co-doped cubic  $\text{NaYF}_4$  NPs by drop-wise transferring sodium and lanthanide trifluoroacetates into the 310  $^\circ\text{C}$  solution (Figure 3A). It is important to note that not only Na(TFA) is decomposed at an extremely high rate, but also do RE trifluoroacetates. Thus, reactions 1 and 2 vigorously take place, generate a burst nucleation, and finally form well-defined cubic RE-doped  $\text{NaYF}_4$  nanoparticles. The nucleation rate of Reaction 1 and 2 in "hot-injection method" is much higher than that in "heating-up" method, which also is the major difference among these two methods. In addition to this, small hexagonal  $\text{NaYF}_4$  nanoparticles can be produced using "hot-injection method", which is not so facile in "heating-up method". Sun group systematically investigated the growth mechanism of  $\text{NaYF}_4$  nanocrystals using "hot-injection" method [42]. When

compared with the classical heating-up approach, they found that the cubic-to-hexagonal phase transformation of  $\text{NaYF}_4$  nanocrystals is significantly accelerated in "hot-injection" method (Figure 3B); and the phase transformation process can be tuned by the injecting temperature. This is because higher reaction rates in all the reactions (1)-(4) are simultaneously realized using "hot-injection method". Hence, small and uniform hexagonal  $\text{NaYF}_4$  nanoparticles can be produced.

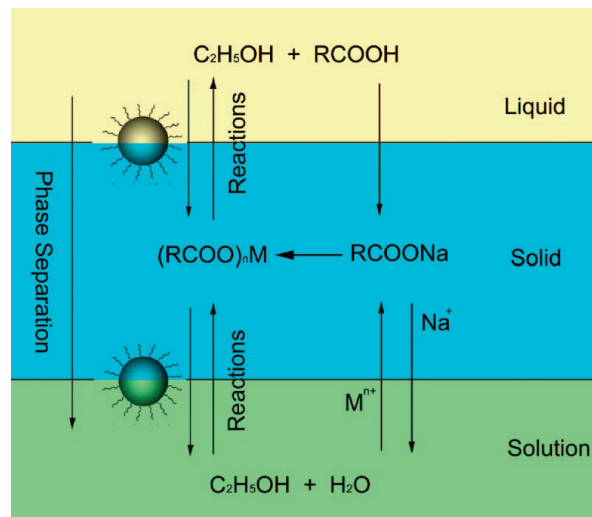
## 2.2 Hydro(solvo)thermal Method

Hydro(solvo)thermal methods perform chemical reactions in a solvent above its critical point under an elevated pressure and temperature, which is enabled by placing RE precursors in aqueous or organic solvents in a sealed and heated autoclave [60-62]. Compared with the thermal decomposition method, hydrothermal synthesis can occur at a lower reaction temperature (general below 200  $^\circ\text{C}$ ) and implement a set of reactions at the same time. Li's group [63] reported a general liquid solid and solution (LSS) approach for the synthesis of nanomaterials, whereby the reaction, phase transfer and separation take place at the interfaces. Taking the preparation of cubic  $\text{NaYF}_4$  nanocrystals (Figure 3) as an example, they primarily added linoleic acid, NaOH, ethanol and deionized water into the vessel, and then add drop-wise the  $\text{Y}(\text{NO}_3)_3$  and NaF solution. After stirring, three phases would be formed, i.e., sodium linoleate (solid), ethanol and linoleic acid (liquid), and the water/ethanol (solution). The phase transfer reaction involves ion exchange of the RE ions spontaneously across the interface of sodium linoleate (solid) and the water/ethanol solution (solution). After the phase transfer process, the RE ions will shift from the aqueous solution into the solid phase, the  $\text{RE}^{3+}$  ions

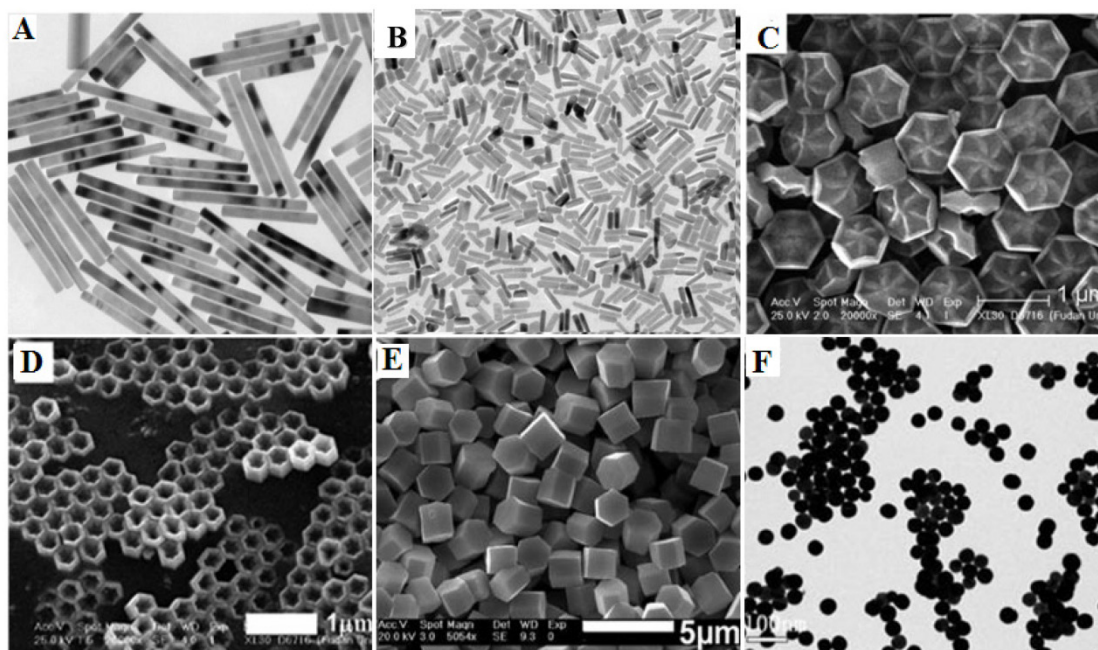
can react with NaF to yield cubic  $\text{NaYF}_4$  nanocrystals.

The LSS method has been proven to be a very powerful to fabricate rare-earth doped  $\text{NaYF}_4$  with diverse morphologies such as, microprism crystals [64], microrods [65], microtubes [66] octahedrons [67], microspheres [68] and flower-like NPs [69]. It is important to note that the doping concentration also has a significant effect on the morphology and phase of final product. For instance, the high Gd-doping concentration can lead the  $\text{NaYF}_4$  particle size to become smaller, while transforming the phase from cubic to hexagonal due to the change in the surface polarization (Figure 5A) [70]. Zhao *et al.* reported the uniform flower-like and tubelike  $\text{NaREF}_4$  arrays (Figure 5C, D) with multicolour UC properties via an oleic acid-assisted hydrothermal method [71]. Li and co-workers used trisodium citrate as complex agent to synthesize diverse shaped  $\text{NaYF}_4$  nanomaterials (Figure 5E) [72]. Recently, our group successfully developed this method to prepare  $\text{BaYF}_5$  NPs using EDTA as chelating agent, revealing that the nucleation process of  $\text{BaYF}_5$  NPs is governed by the pH-sensitive chelating ability of EDTA with both  $\text{Ba}^{2+}$  and  $\text{Ln}^{3+}$  (Figure 5F) [73]. Though hydrothermal (solvo) method is able to produce nanoparticles of vary-

ing type, shape and size, it generally takes a long time (e.g., 24 hours) to produce uniform monodispersed nanoparticles. In addition, it requires to use strict reaction conditions to produce smaller size nanoparticles, as hydro(solvo)thermal method prefers to grow particles in bigger size.



**Figure 4.** Schematic of liquid–solid–solution (LSS) phase transfer and separation synthesis. Reproduced with permission from reference [63].



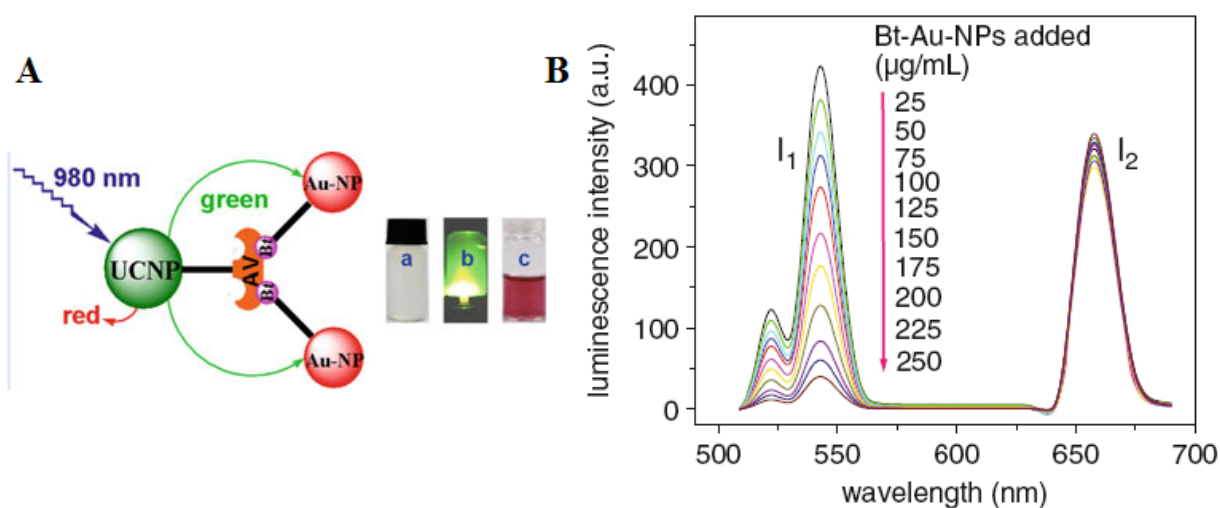
**Figure 5.** Different shapes of RE-doped fluoride nano-/microcrystals by hydro(solvo)thermal method. Reproduced with permission from references [70-73].

### 3. Sensing Using RE-Doped Upconversion Nanoparticles

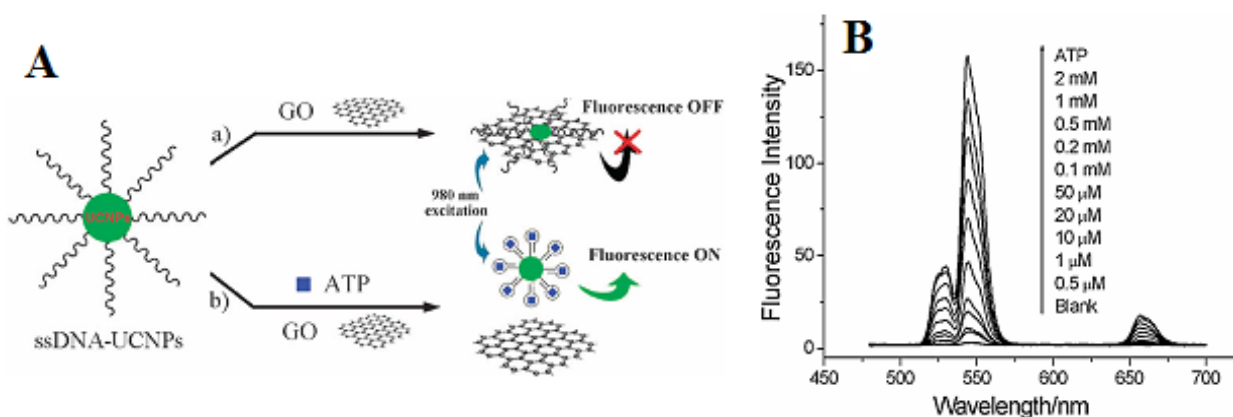
#### 3.1. Applications in Biomolecules Sensing

It is well known that biomolecules analysis is of great importance in biological detection, genetic, and molecular medicine. Detection of biomolecules via UCNPs as luminescent reporters in a variety of in vitro assays appears to be one of the most attractive approaches, as it works at virtually zero background and thus improved the limits of detection (LOD) when compared with conventional reporters (e.g., dyes, quantum dots). In the early age of sensing applications, Hampl *et al.* utilized sub-micron-sized  $\text{Y}_2\text{O}_3\text{:Yb/Er}$  particles as UC luminescent transducer [74]. Despite of the large size, they still show a low LOD of 10 pg human chorionic gonadotropin in a lateral flow (LF) immunochromatographic assay, which is about  $\sim 10$ -fold increase over the use of conventional labeling agents of colloidal gold or colored latex beads. Similarly, Tanke *et al.* used 400-nm  $\text{Y}_2\text{O}_3\text{:Yb/Er}$  particles to obtain a low LOD of 1 ng/ $\mu\text{l}$  oligonucleotides [75]. It was found that the sensitivity is 4 times stronger than the one using the conventional reporter of cyanine 5 labels. Recently, utilizing small but efficient upconversion nanoparticles, biomolecules sensors based on upconversion FRET technique have also been proven to exhibit a high sensitivity in a range of biological and chemical analyses [76]. A FRET system comprise of fluorescence donor and acceptor, which are conjugated to different biomolecular entities. The fluorescence of the donor can be effectively quenched (absorbed) by the acceptor

when the distance of the donor and the acceptor comes into nanometer scale. As the distance of the donor and the acceptor is determined by their concentrations, the fluorescence intensity is linearly related to the concentration of the target when fixing either a donor or an acceptor concentration. Importantly, the FRET-UCNPs system was proved to have quite low LOD in a range of experiments [77-52]. Wang *et al.* [77] firstly exploited the FRET system using UCNPs as energy donors and gold NPs as energy acceptors to detect goat antihuman immunoglobulin (IgG), reaching a low LOD of 0.88 mg/mL. Moreover, Soukka group has shown that UCNPs are useful in energy transfer-based sandwich immune assays [78,79]. Subsequently, Wolfbeis's group developed the FRET system employing the acceptor of biotinylated Au-NPs and the donor of the avidin-modified  $\text{NaYF}_4\text{:Yb/Er}$  NPs in order to detect trace amounts of avidin [80]. The scheme of the FRET system in their work is shown in Figure 6A. When Au-biotin NPs were added into the solution of avidin-conjugated UCNPs, it will bond to the surface of the UCNPs due to the sensitive and selective interaction between avidin and biotin. Since the strong absorption at  $\sim 541$  nm of Au NPs well matches the UC emission of  $\text{NaYF}_4\text{:Yb}^{3+}, \text{Er}^{3+}$  NPs, the green emission in UC nanoparticles will be quenched due to the FRET process. A resulted linear quenching of green UC emissions allows us to detect trace amounts of avidin proteins. Li group used a similar approach to detect avidin on the basis of the selective binding of avidin and biotin [81], displaying the ability to detect an amount of avidin in "nM".



**Figure 6.** (A) Schematic representation of the binding of biotinylated gold nanoparticles to avidinylated UCNPs. Photographs: (a) colorless suspension of UCNP under visible light; (b) UCNP with green luminescence under 980-nm laser excitation; (c) adding red Au-NPs under visible light. (B) Luminescence of the UCNPs (photo-excited at 980 nm) after addition of varying concentrations of biotinylated gold NPs. Adapted from reference [80].



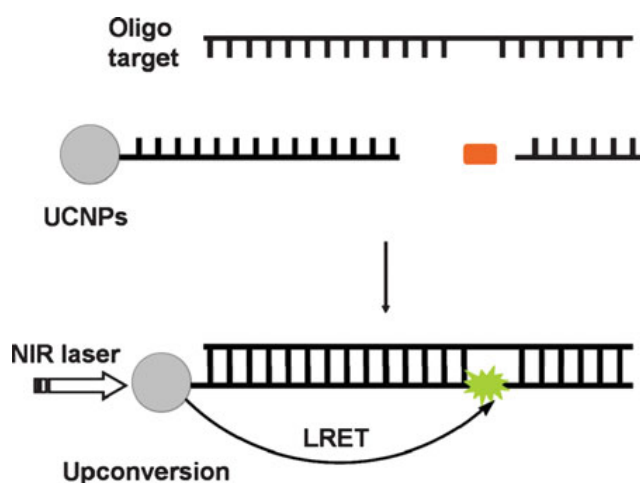
**Figure 7.** (A) Schematic illustration of the upconversion FRET process between ssDNA-UCNPs and GO for ATP sensing; (B) PL spectra of the UCNPs-GO FRET aptasensor of varying concentrations of ATP. Adapted from reference [82].

Instead of using gold as an acceptor, Liu *et al.* proposed a novel FRET sensor platform utilizing graphene oxide as an acceptor [82]. In this system, Yb/Er-codoped NaYF<sub>4</sub> UCNPs were conjugated to ssDNA; their whole visible upconversion emissions were totally quenched by graphene oxide (GO) due to their ultrahighly strong absorption, as shown in Figure 7. When adding the adenosine triphosphate (ATP), their luminescence can be recovered by gradual dissolution of them from GO. Luminescence increase of single-stranded DNA-functionalized UCNPs (ssDNA-UCNPs) was found to be linearly dependent on the concentration of ATP (Figure 7A). It is striking that this result not only was performed in a wide detection range from 0.5 μM to 2 mM (Figure 7B), but also extends the application of UCNPs biosensors to the DNA biomolecules [83].

In addition, UCNPs-based sensing technique can also be used for the detection of oligonucleotides [84], as displayed in Figure 8. The longer target nucleotide can be formed by two short oligonucleotides, which respectively attached to a UCNP and a fluorophore. When the targeted oligonucleotides are produced, the efficient luminescent resonance energy transfer (LRET) process from the UCNP to the fluorophore takes place, evoking fluorescence from the fluorophore.

An aptasensor based on magnetic NPs coupled with UCNPs for specific detection of bacteria of *S. Typhimurium* and *S. aureus* was also explored by Duan *et al.* [85]. This design allows one to capture and concentrate bacteria with the help of a magnetic field, and monitor the process by the amplified luminescent signal due to accumulation. Besides gold, GO, and magnetic NPs, Shao's group also explore FRET bio-sensing system based on the silver NPs and the UCNPs for DNA detection [86]. These recent sensing

works suggests that UCNPs (often used RE-doped NaYF<sub>4</sub> nanomaterials) with proper biomolecules-targeting can apply to different biomolecules detection.



**Figure 8.** The schematic of an oligonucleotide sensor design. Reproduced with permission from reference [84].

### 3.2. Applications in Ions Sensing

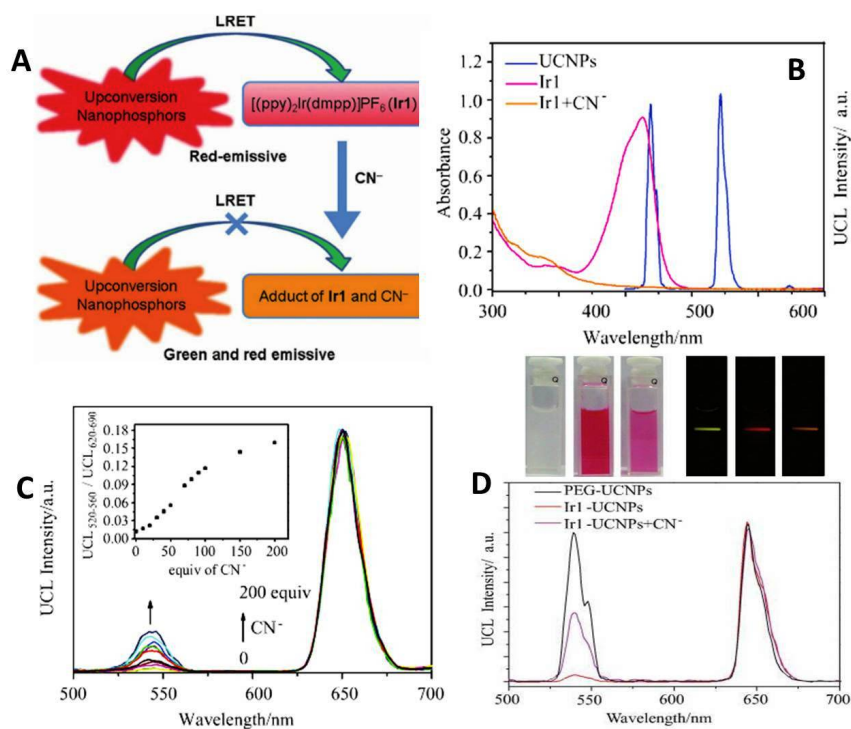
In this section, we summarized recent works on the use of UCNPs for detecting various chemical ions, which delivers real-time information on targeted ions in complex samples. Hazardous ions such as cyanide ions (CN<sup>-</sup>) and mercuric ions (Hg<sup>2+</sup>) are extremely toxic to mammals [87]; detecting and evaluation of the concentration of these, therefore, are of particular interests and importance for the lives. Sensing ions using UC lanthanide-doped UCNPs has been shown to be highly sensitive in living cells due to efficient LRET [30]. As the UC effect is inert to the interested ions

[32], UCNPs have to be used in combination with suitable indicator that has a recognition capability of the targeted ions. The biochemical recognition will then modulate the fluorescence intensity of UCNPs and make the luminescent intensity dependent on the targeted ion concentration. In such way, the UCNPs can perform an accurate detection of the targeted ions; the displayed colorimetric changes in solution even can be discerned by the naked eye [88].

Li *et al.* reported on a highly selective and sensitive  $\text{CN}^-$  sensor by using a chromophoric iridium (III) complex-coated UCNP. This sensing system relies on the strong quenching of the green UC emission by chromophoric iridium (III) complex due to the LRET mechanism [89]. When adding  $\text{CN}^-$ , the quenching effect dramatically decreases and causes LRET to be ineffective. Hence, the green UC emission of NPs can be recovered (Figure 9A). The emission spectrum of the UCNPs and the absorption spectrum of Ir1 are shown in Figure 9B. The UC emission peaks at 540 nm and 650 nm. The Ir1 dye has a strong absorbance with a maximum peak at 530 nm, which does not influence the red emission band of UCNPs. When  $\text{CN}^-$  complex is absent in the system, chromophoric iridium (III) complex exerts a significant quenching effect on green band of the UCNPs. As the absorption of chromophoric iridium (III) complex at  $\sim 500$  nm is quite sen-

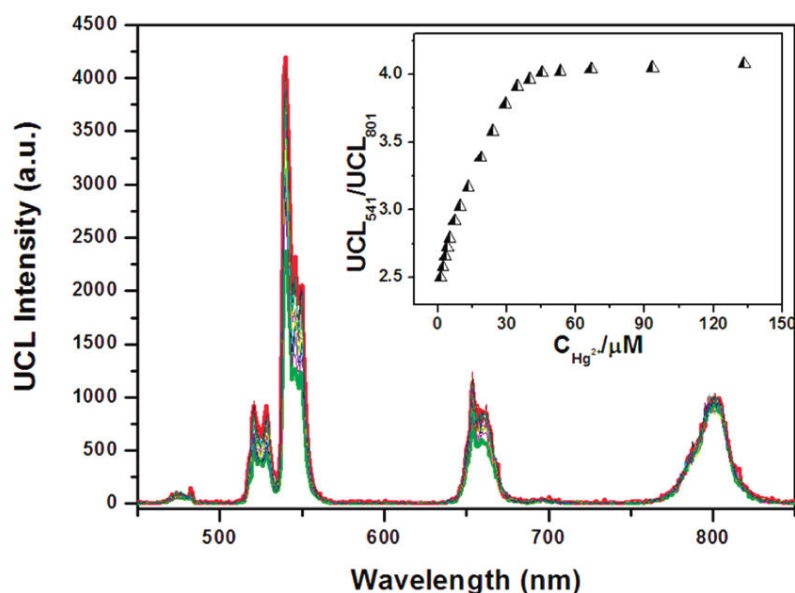
sitive to the  $\text{CN}^-$  ions, this feature creates a possibility to use ratiometric evaluation  $\text{CN}^-$  concentration using the green UC at 540 nm and red UC at 650 nm (its intensity is not affected by  $\text{CN}^-$  ions). The UC luminescence spectra at different concentration of  $\text{CN}^-$  values are shown in Figure 9C. The ratiometric change of intensity between green emissions at 540 nm and red at 650 nm clearly has a linear dependence on the  $\text{CN}^-$  concentration. It is important to note that the developed  $\text{CN}^-$  sensor was implemented in pure water, having an important implication for use in live cells [32].

In another work by Li's group, chromophoric ruthenium complex-assembled UCNPs were prepared to detect  $\text{Hg}^{2+}$  ions [88]. They employed  $\text{NaYF}_4:20 \text{ mol\% Yb}, 1.6 \text{ mol\% Er}, 0.4 \text{ mol\% Tm}$  UCNPs which are coated with the ruthenium complex that is sensitive to  $\text{Hg}^{2+}$  ions. They use the ratio ( $\text{UCL}_{541}/\text{UCL}_{801}$ ) as the output signal to detect the  $\text{Hg}^{2+}$  in aqueous solution, as the intensity of the 801 nm emission is immune to the  $\text{Hg}^{2+}$  ions. The experimental result is shown in the inset of Figure 10. The LOD of  $\text{Hg}^{2+}$  ions for this sensor in water was down to 1.95 ppb (parts per billion); this value is even lower than the maximum level (2 ppb) of  $\text{Hg}^{2+}$  in drinking water set by the United States Environmental Protection Agency.



**Figure 9.** (A) Schematic illustration of the LRET process between UCNPs and the iridium(III) complex  $[(\text{ppy})_2\text{Ir}(\text{dmpp})]\text{PF}_6$ , Ir1. (B) UV-vis absorption spectra of Ir1 and Ir1 upon addition of  $\text{CN}^-$ , and photoluminescence spectrum of UCNPs. (C) Emission intensity changes of the Ir1-UCNPs complex with an increasing amount of cyanide in water. Inset illustrates the change of the intensity ratio (the emission band at 520 nm to the 650 nm emission band) as a function of the  $\text{CN}^-$  concentration. (D) Photographs of water solutions of PEG-UCNPs, Ir1-UCNPs and Ir1-UCNPs after doped in 500 equiv. of  $\text{CN}^-$  (top left); corresponding photographs of emission (top right) and photoluminescence spectra (bottom) with an excitation at  $\sim 980$  nm. Reproduced with permission from reference [89].





**Figure 10.** Upconversion luminescence spectra of  $0.3 \text{ mg mL}^{-1}$  N719-UCNPs ( $27.6 \text{ }\mu\text{M}$  N719) in the aqueous solution upon a gradual addition of  $Hg^{2+}$  ions (from 0 to  $135 \text{ }\mu\text{M}$ ). Inset: the ratio  $UCL_{541}/UCL_{801}$  of upconversion luminescence intensities at 541 and 801 nm of N719-UCNPs as a function of  $Hg^{2+}$  concentration. Reproduced with permission from reference [88].

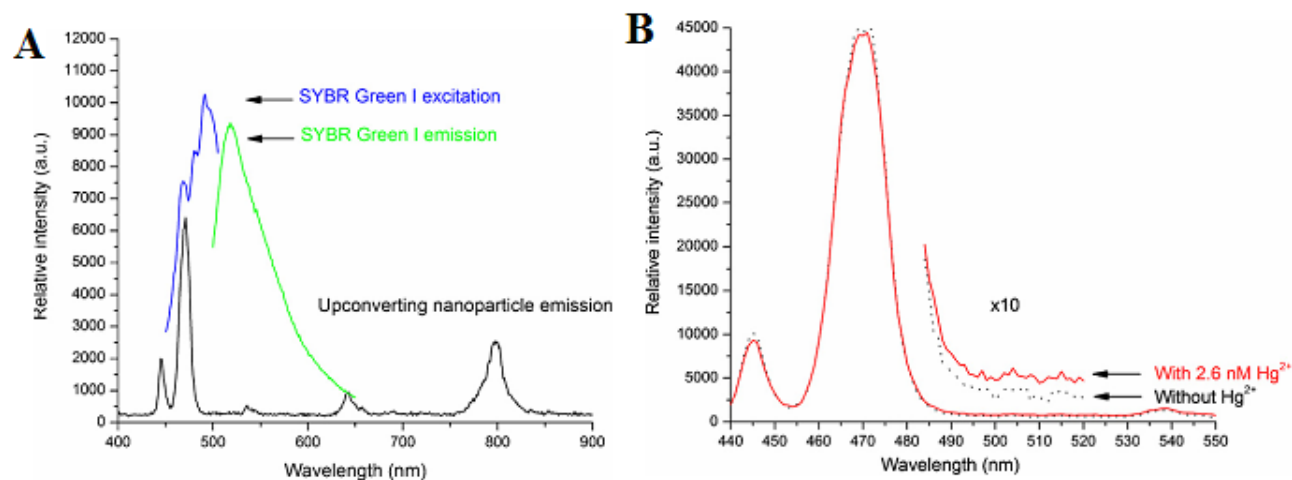
Differing from Li's work, Zhang *et al.* proposed a new scheme for detecting  $Hg^{2+}$  in aqueous media through the use of a single-stranded DNA as  $Hg^{2+}$ -capturing element [90]. A  $NaYF_4:Yb/Tm$  UC NP is employed as an energy donor, while the SYBR dye functions as an energy acceptor. As shown in Figure 11A, the SYBR has a strong absorbance overlapping with the visible blue emission of the UCNPs around 477 nm. After the addition of  $Hg^{2+}$  ion, the luminescence spectra of the mixture are shown in Figure 11B. This result indicated the energy transfer between the UCNPs and SYBR causes simultaneous decrease of the 477 nm emission of the UCNPs and the increase of signals corresponding to SYBR green emission. Utilizing the ratio of the acceptor emission to the donor emission, mercuric ions can be quantified with a high sensitivity at a LOD of 0.06 nM. Yan's group developed a novel approach for the detection of  $Ce^{4+}$  by MPTEA-functionalized UCNPs derived from azelaic aldehyde-capped precursors [91]. And the  $Ce^{4+}$  sensor was constructed based on the dual-emission arising from different spectral responses of MPTEA and the UCNPs. To sum up, these UCNPs functionalized with other groups have great potential for applications in ions sensing.

### 3.3. Applications in Gas Molecules Sensing

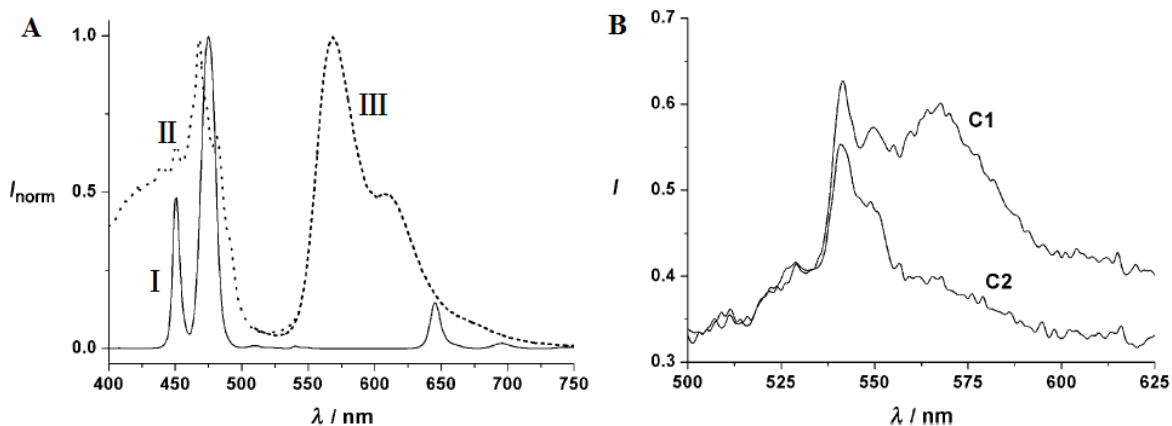
Determination of gas molecules such as oxygen, carbon dioxide, ammonia, and many others in aque-

ous samples or biological fluids has great significance in analytical biochemistry, clinical medical diagnosis and bioprocess monitoring [92,93]. The use of UCNPs for gas molecules sensing has attracted extensive interest because of their outstanding properties [28, 94]. The first sensor based on UCNPs of oxygen was presented by Wolfbeis group [94], in which UCNPs as nanolamps and iridium(III) complexes as quenchers were both embedded in a thin film of ethyl cellulose. The emission of the UCNPs overlaps with the absorbance of the iridium(III) complex (Figure 12A). Thus, the green-yellow luminescence of iridium complex can be induced by the blue emission of  $NaYF_4:Yb,Tm$  UCNPs when excited at  $\sim 980 \text{ nm}$ . Since the fluorescence of iridium(III) complex is sensitive to molecular oxygen, its intensity is sensitive the content of environmental oxygen (Figure 12B).

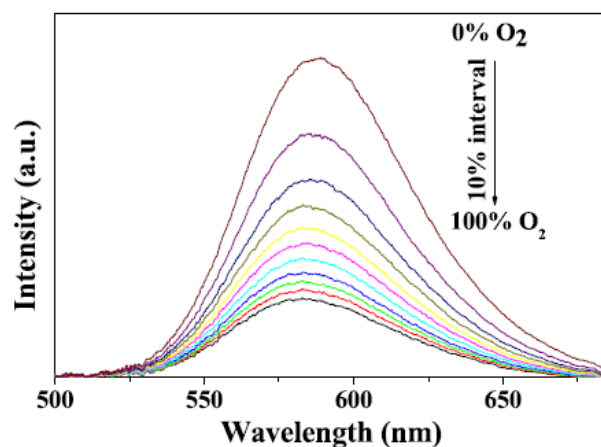
Liu *et al.* [95] designed a novel multifunctional nanocomposite sensor, which possesses upconversion, oxygen-sensing and bio-affinity properties. The UCNPs of the type  $NaYF_4:Yb,Tm$  coated with Ru(II) complex chemically doped silica form the sensor to obtain the response to oxygen. When the multifunctional sensor was exposed to  $O_2$ , the emission intensity of the Ru(II) complex decreased. Furthermore, the novel oxygen sensor carried out the precise detection from 0 to 100%  $O_2$ , indicating its high sensitivity (Figure 13).



**Figure 11.** (A) Photoluminescence spectrum of the NaYF<sub>4</sub>:Yb<sup>3+</sup>,Tm<sup>3+</sup> nanoparticles, excited by a 980 nm diode laser, and the excitation and emission spectra of SYBR Green I are included for comparison. (B) Photoluminescence spectra of the photon UCNPs before (dark) and after (red) the addition of 2.6 nM of Hg ions, in the presence of SYBR Green I (~2 μM) and PDCA (~6.8 mM). Reproduced with permission from reference [90].

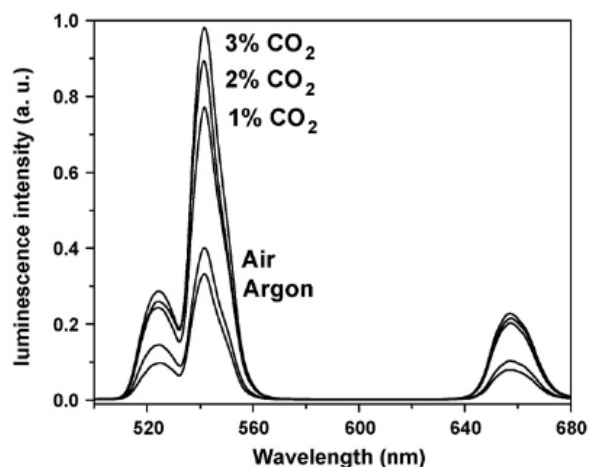


**Figure 12.** (A) Emission spectra of the NaYF<sub>4</sub>:Yb,Tm nanoparticles (i), the absorption of the oxygen probe [Ir(CS)<sub>2</sub>(acac)] (ii), emission spectrum of [Ir(CS)<sub>2</sub>(acac)] (iii); (B) Visible emission spectra of an ethyl cellulose sensor film containing the NaYF<sub>4</sub>:Yb,Tm UCNPs and the oxygen probe [Ir(CS)<sub>2</sub>(acac)]; (C1) in argon and (C2) argon containing 20% oxygen. Reproduced with permission from reference [94].



**Figure 13.** Room temperature emission spectra of Ru(II) complex functionalized NaYF<sub>4</sub>:Yb<sup>3+</sup>,Tm<sup>3+</sup>@SiO<sub>2</sub> under different oxygen concentrations. Reproduced with permission from reference [95].

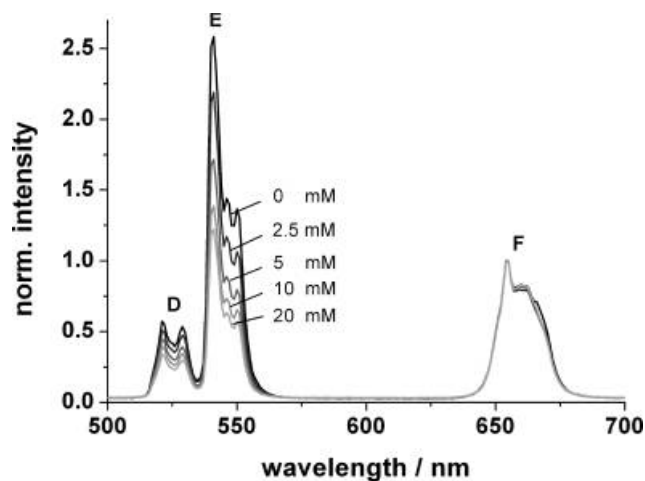
Sun *et al.* presented the first optical pH sensor based on UC luminescence of NaYF<sub>4</sub>:Yb/Er nanorods and pH dependent absorption spectrum of BTB (bromothymol blue), which can be extended to sense acidic gases such as (dissolved) carbon dioxide or (dissolved) ammonia [96]. Subsequently, the carbon dioxide and ammonia optical sensors have been developed based on the colorimetric or fluorometric changes due to the resulted variation of pH value in solution induced by these gas molecules [97, 98]. Usually, optical sensors for CO<sub>2</sub> and NH<sub>3</sub> are based on their reactions with hydroxy ions of an alkaline buffer. The change in the pH value leads to the change in color or fluorescence of the indicator. Thus, CO<sub>2</sub> and NH<sub>3</sub> sensing experiment can be carried out by detecting the variation of luminescence intensity of UCNP. Wolfbeis group has developed a novel CO<sub>2</sub> optical sensors, which coupled NaYF<sub>4</sub>:Yb,Er UCNP with BTB in a matrix of polystyrene [99]. The polystyrene as matrix displays high permeation to CO<sub>2</sub> but rejection to protons. As CO<sub>2</sub> penetrated the polymer and reacted with hydrated BTB ion pair, the pH inside the film decreased, leading the emission of the UCNP to increase. As shown in Figure 14, the detection of CO<sub>2</sub> can range from 0 to 3%. The response time is evaluated to be about 10 s for switching from pure argon gas to 1% CO<sub>2</sub> in argon, and the LOD is measured to be about 0.11% for the content of CO<sub>2</sub>.



**Figure 14.** Upconversion emission spectra of the polystyrene sensor film containing the UCNP in presence of 1, 2 and 3% of CO<sub>2</sub>, air (0.003% CO<sub>2</sub>) and argon. Reproduced with permission from reference [99].

According to a similar principle, Mader *et al.* [28] has designed an ammonia sensor based on the combination of NaYF<sub>4</sub>:Yb,Er nanoparticles and a pH probe of the phenol red which are both immobilized in a polystyrene matrix. Once the NH<sub>3</sub> penetrated the

sensor film, it produced a strong absorption at 560 nm in the pH probe; the green emission of the UCNP will then be screened off. Since the emission band at 660 nm is not affected by the indicator dye, its intensity can serve as a reference standard. The ratio of the intensities of the green and the red UC emission, therefore, can be used to determine the content of ammonia. Figure 15 displays the decrease of the intensity of the green emission band along an increase in the ammonia concentration from 0 to 20 mM; the LOD of this system was evaluated to be as low as 400 μM.



**Figure 15.** Upconversion luminescence spectra of the ammonia sensor film at dissolved ammonia concentrations between 0 and 20 mM. Excitation wavelength 980 nm; spectra are normalized to the peak at 655 nm. Reproduced with permission from reference [28].

### 3.4. Applications in Temperature Sensing

Temperature (*T*) is a fundamental parameter, which plays an important role for numerous applications and scientific researches [100]. An accurate and non-invasive determination of this parameter is also of particular importance for biology, for example, the investigation of enzyme reactions or metabolism in single live cell. Fluorescence intensity ratio (FIR) of the emission of lanthanide ions has been proposed for temperature measurement as early as 1976 by Kusama *et al.* [101]. This technique relies on that the intensities from two emitting levels of lanthanides have strong dependences on temperature. Among lanthanide ions, the emissions of Er<sup>3+</sup> ions at 530 nm from the <sup>2</sup>H<sub>11/2</sub>→<sup>4</sup>I<sub>15/2</sub> and at 550 nm from the <sup>4</sup>S<sub>3/2</sub>→<sup>4</sup>I<sub>15/2</sub> transition is of particular interest for this endeavor, as the populations in <sup>4</sup>S<sub>3/2</sub> and <sup>2</sup>H<sub>11/2</sub> levels follow the Boltzmann Distribution Law when using steady-state excitation. The two intensities of *I*<sub>520</sub> and *I*<sub>550</sub> relate to the temperature *T* through the following mathematical equation [102],

$$\frac{I_{520}}{I_{550}} = A \exp\left(-\frac{\Delta E}{K_b T}\right) \quad \dots(5)$$

where  $K_b$  is the Boltzman constant,  $\Delta E$  is the energy gap between the two excited levels and  $A$  is a constant. Equation (5) illustrates that the logarithmic ratio of  $I_{520}/I_{550}$  has a linear dependence on the inverse of temperature. It is also important to note that  $\text{Er}^{3+}$  ions can have good upconversion emissions at 530 and 550 nm when excited at wavelength of 980 nm that falls within the "optical transmission window of tissue". This feature provides an opportunity for non-invasive and sensitive measurement of temperature in biological processes, even for that located at deep tissues [103]. In addition, the ratiometric data of  $I_{520}/I_{550}$  are independent of variations in the intensity of the laser excitation source and drifts in the photodetector, making them ideally suited for temperature sensing. While optical temperature sensors utilizing the intensity ratio of  $I_{520}/I_{550}$  in  $\text{Er}^{3+}$  ions have been extensively investigated [103-106], most studies were based RE doped oxide bulk materials that are incompatible with biology. A use of optical temperature sensors in biology requires colloidal small-sized RE-doped nanoparticles with highly efficient upconversion nanoparticles.

Fluoride materials have been proved to be more efficient than oxide materials due to their low phonon cut-off energy [107-110].  $\text{Yb}^{3+}$  ion has a very large absorption cross-section at  $\sim 976$  nm, which also can efficiently sensitize the neighboring  $\text{Er}^{3+}$  ions and dramatically increase the upconversion emissions.  $\text{Yb}/\text{Er}$ -codoped colloidal fluoride nanoparticles, therefore, become a promising nanothermometer for use in biology. The temperature dependence of  $\text{Yb}/\text{Er}$  codoped  $\text{NaYF}_4$  powders were investigated independently by Suyver *et al.* [110] and Wu *et al.* [111], drawing the same conclusion as described in equation (5). Although  $\text{Tm}^{3+}/\text{Yb}^{3+}$  codoped  $\text{Y}_2\text{O}_3$  UCNPs were investigated as thermometers to detect a temperature range from 303 K to 753 K [112], the sensitivity of temperature (a fractional rate of change in the fluorescence intensity ratio with the temperature) is lower than  $\text{Er}^{3+}/\text{Yb}^{3+}$ -doped fluoride nanoparticles. The first real UC nanothermometer in live cell was demonstrated by Capobianco *et al.* using water-dispersed polyethyleneimine-coated  $\text{NaYF}_4:\text{Er}^{3+}/\text{Yb}^{3+}$  UCNPs (Figure 16C) [113]. To demonstrate their ability to record thermal gradient images of liquids, nanothermometers were first used to obtain thermal profiles in a water solution of  $\text{NaYF}_4:\text{Er}^{3+}/\text{Yb}^{3+}$  nanoparticles using a pump-probe experiment (Figure 16 A and B). When excited at 980

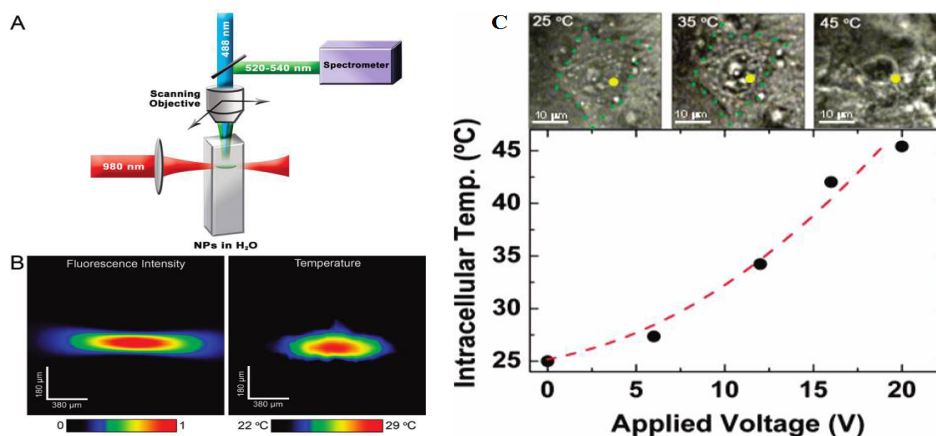
nm (pump beam) the total emission fluorescence intensity of these nanoparticles was used to reveal the pump shape profile (see Figure 16B, left panel). Simultaneously, the small-sized focus point of 488 nm ( $\text{Ar}^+$ ) laser (probe beam) was scanning over the pump beam profile to accurately determine the fluorescence intensity ratio of  $I_{525}/I_{545}$ , and thus the temperature of each point on the pump profile (see Figure 16B, right panel). In another experiment, following incubation of the  $\text{NaYF}_4:\text{Er}^{3+}/\text{Yb}^{3+}$  nanoparticles with HeLa cervical cancer cells and their subsequent uptake, the fluorescent nanothermometers were used to measure the internal temperature of the living cell from 25 °C to its thermally induced death at 45 °C, as shown in Figure 16C. It is important to note that the excitation wavelength in Figure 16C is  $\sim 920$  nm; this wavelength is not absorbed by water and creates negligible thermal effects. Experiments in Figures 16 conclusively demonstrate that the  $\text{NaYF}_4:\text{Er}^{3+}/\text{Yb}^{3+}$  nanoparticles are good nanothermometers for biology. We would like to point out that Wolfbeis *et al.* have investigated temperature sensing using UCNPs of varying size and RE dopants recently [114]. They found that the core-shell structured hexagonal ( $\text{NaYF}_4:\text{Yb}20\%\text{Er}2\%$ )/ $\text{NaYF}_4$  UCNPs, due to their higher brightness, are more suitable for temperature sensing, as they have the ability to resolve temperature differences of less than 0.5 °C in the physiological range between 20 and 45 °C [114]. Nanoparticle-based thermometer offers many options for imaging the two-dimensional distribution of temperature, and plays a vital role for understanding the sub-cellular processes. Applications of UCNPs in a range of other nanophotonic and biophotonic topics can be found in a recent review [115].

#### 4. Conclusions

This review summarizes recent progresses on the chemical synthesis and sensing applications of UCNPs. Novel sensing strategies are always based on the development of materials science with new and novel properties. The unique frequency converting properties in monodisperse UCNPs indeed provided numerous opportunities for a wide range of theranostic applications, such as detection of biomolecules (e.g., avidin, ATP, *etc.*), ions (cyanide, mercury, *etc.*), small gas molecules (oxygen, carbon dioxide, ammonia, *etc.*), as well as *in vitro* temperature sensing. However, challenges are still remained, for example, the aqueous phase UCNPs with high efficiency are required for biological sensors. Although surface engineering can impart water solubility and biocompatibility to them, the luminescence efficiency after surface modification generally decreases a lot. In ad-

dition, a practical sensing application requires UCNPs to be highly efficient, while the biology requires UCNPs to be as small as possible to reduce any exposed potential toxicity to the body. However, small size generally results in very low luminescence efficiency, especially for the size below 10 nm. Ways to

increase the upconversion efficiency as well as applications of UCNPs in piratical medical problems need to be explored, which are expected to result in better sensing sensitivity and ultimately provide ways for point of care of diagnosis of diseases.



**Figure 16.** (A) Schematic of nanothermometer used to monitor the temperature profile created by heating a colloidal solution of  $\text{NaYF}_4:\text{Er}^{3+}, \text{Yb}^{3+}$  UCNPs in water with a NIR diode laser (980 nm, pump beam) and scanned with a  $\text{Ar}^+$  laser (488 nm, probe beam). (B) Confocal image of all the visible upconverted luminescence under 980 nm excitation (Left). Thermal image of the spot created by the 980 nm pump beam (Right). (C) Optical transmission images of an individual HeLa cell at different temperatures and temperature-dependent property of the HeLa cell determined by UCNPs as a function of the applied voltage [113]. The voltage determines the heating temperature of plate under the cells. Reproduced with permission from reference [113].

## Acknowledgment

This work is supported by Natural Science Foundation of China (51102066).

## Competing Interests

The authors have declared that no competing interest exists.

## References

- Auzel F. Upconversion and anti-Stokes processes with f and d ions in solids. *Chem Rev.* 2004; 104: 139-74.
- Auzel F. Upconversion processes in coupled ion systems. *J Lumin.* 1990; 45: 341-45.
- Wang F, Liu XG. Recent advances in the chemistry of lanthanide-doped upconversion nanocrystals. *Chem Soc Rev.* 2009; 38: 976-89.
- Haase M, Schäfer H. Upconverting Nanoparticles. *Angew Chem Int Ed.* 2011; 50: 5808-29.
- Achatz DE, Ali R, Wolfbeis OS. Luminescent Chemical Sensing, Biosensing, and Screening Using Upconverting Nanoparticles. *Top Curr Chem.* 2011; 300: 29-50.
- Wang F, Banerjee D, Liu YS, Chen XY, Liu XG. Upconversion nanoparticles in biological labeling, imaging, and therapy. *Analyst.* 2010; 135: 1839-54.
- Longmire M, Choyke PL, Kobayashi H. Clearance properties of nano-sized particles and molecules as imaging agents: considerations and caveats. *Nanomedicine.* 2008; 3: 703-17.
- Wang F, Deng RR, Wang J, Wang QX, Han Y, Zhu HM, Chen XY, Liu XG. Tuning Upconversion through Energy Migration in Core-Shell Nanoparticles. *Nat Mater.* 2011; 10: 968-73.
- Liu YS, Tu DT, Zhu HM, Li RF, Luo WQ, Chen XY. A Strategy to Achieve Efficient Dual-Mode Luminescence of  $\text{Eu}^{3+}$  in Lanthanides Doped Multifunctional  $\text{NaGdF}_4$  Nanocrystals. *Adv Mater.* 2010; 22: 3266-71.
- Yi GS, Peng YF, Gao ZQ. Strong Red-Emitting near-Infrared-to-Visible Upconversion Fluorescent Nanoparticles. *Chem Mater.* 2011; 23: 2729-34.
- Pichaandi J, Boyer JC, Delaney KR, van Veggel FCJM. Two-Photon Upconversion Laser (Scanning and Wide-Field) Microscopy Using  $\text{Ln}^{3+}$ -Doped  $\text{NaYF}_4$  Upconverting Nanocrystals: A Critical Evaluation of their Performance and Potential in Bioimaging. *J Phys Chem C.* 2011; 115: 19054-64.
- Suyver JF, Grimm J, Krämer KW, Güdel HU. Upconversion spectroscopy and properties of  $\text{NaYF}_4$  doped with  $\text{Er}^{3+}$ ,  $\text{Tm}^{3+}$  and/or  $\text{Yb}^{3+}$ . *Luminescence.* 2006; 117: 1-12.
- Li CX, Lin J. Rare earth fluoride nano-/microcrystals: synthesis, surface modification and Application. *J Mater Chem.* 2010; 20: 6831-47.
- Wang ZL, Chan HLW, Li HL, Hao JH. Highly efficient low-voltage cathodoluminescence of  $\text{LaF}_3:\text{Ln}^{3+}$  ( $\text{Ln}=\text{Eu}^{3+}, \text{Ce}^{3+}, \text{Tb}^{3+}$ ) spherical particles. *Appl Phys Lett.* 2008; 93: 141106.
- Chen GY, Ohulchanskyy TY, Kumar R, Ågren H, Prasad PN. Ultrasmall Monodisperse  $\text{NaYF}_4:\text{Yb}^{3+}/\text{Tm}^{3+}$  Nanocrystals with Enhanced Near-Infrared to Near-Infrared Upconversion Photoluminescence. *ACS Nano.* 2010; 4: 3163-68.
- Liu Q, Sun Y, Yang TS, Feng W, Li CG, Li FY. Sub-10 nm Hexagonal Lanthanide-Doped  $\text{NaLuF}_4$  Upconversion Nanocrystals for Sensitive Bioimaging in Vivo. *J Am Chem Soc.* 2011; 133: 17122-25.
- Yi G, Chow G. Colloidal  $\text{LaF}_3:\text{Yb}, \text{Er}$ ,  $\text{LaF}_3:\text{Yb}, \text{Ho}$  and  $\text{LaF}_3:\text{Yb}, \text{Tm}$  nanocrystals with multicolor upconversion fluorescence. *J Mater Chem.* 2005; 15: 4460-64.
- Mai HX, Zhang YW, Si R, Yan ZG, Sun LD, You LP, Yan CH. High-quality sodium rare-earth fluoride nanocrystals: Controlled synthesis and optical properties. *J Am Chem Soc.* 2006; 128: 6426-36.
- Wang LY, Li YD. Controlled Synthesis and Luminescence of Lanthanide Doped  $\text{NaYF}_4$  Nanocrystals. *Chem Mater.* 2007; 19: 727-34.
- Haase M, Schäfer H. Upconverting Nanoparticles. *Angew Chem Int Ed.* 2011; 50: 5808-29.
- Li CX, Lin J. Rare earth fluoride nano-/microcrystals: synthesis, surface modification and application. *J Mater Chem.* 2010; 20: 6831-47.
- Wang X, Peng Q, Li YD. Interface-mediated growth of monodispersed nanostructures. *Acc Chem Res.* 2007; 40: 635-43.
- Yan ZG, Yan CH. Controlled synthesis of rare earth nanostructures. *J Mater Chem.* 2008; 18: 5046-59.
- Gao FG, Jeevarajan AS, Anderson MM. Long-term continuous monitoring of dissolved oxygen in cell culture medium for perfused bioreactors using optical oxygen sensors. *Biotechnol Bioeng.* 2004; 86: 425-33.

25. Amao Y, Miyashita T, Okura I. Optical oxygen sensing based on the luminescence change of metalloporphyrins immobilized in styrene-pentafluorostyrene copolymer film. *Analyst*. 2000; 125: 871-75.
26. Achatz DE, Meier RJ, Fischer LH, Wolfbeis OS. Luminescent Sensing of Oxygen Using a Quenchable Probe and Upconverting Nanoparticles. *Angew Chem Int Ed*. 2011; 50: 260-63.
27. Shin JH, Lee SH, Kim MH, Yoon HJ, Lee JS, Cha GS, Nam H. Microchip-based pCO<sub>2</sub> gas sensor system with improved analytical performance for point-of-care testing of CO<sub>2</sub> levels in whole blood samples. *Clin Chem*. 2000; 46: A60-A61.
28. Mader HS, Wolfbeis OS. Optical Ammonia Sensor Based on Upconverting Luminescent Nanoparticles. *Anal Chem*. 2010; 82: 5002-5004.
29. Holland MA, Kozlowski LM. Clinical features and management of cyanide poisoning. *Clin Pharm*. 1986; 5: 737-41.
30. Liu JL, Liu Y, Liu Q, Li CY, Sun LN, Li FY. Iridium(III) Complex-Coated Nanosystem for Ratiometric Upconversion Luminescence Bioimaging of Cyanide Anions. *J Am Chem Soc*. 2011; 133: 15276-79.
31. Zheng N, Wang QC, Zhang XW, Zheng DM, Zhang ZS, Zhang SQ. Population health risk due to dietary intake of heavy metals in the industrial area of Huludao city, China. *Sci Total Environ*. 2007; 387: 96-104.
32. Chen J, Xiao JL, Zhao J. Upconversion Nanomaterials: Synthesis, Mechanism, and Applications in Sensing. *Sensors*. 2012; 12: 2415-33.
33. Wang F, Liu XG. Recent advances in the chemistry of lanthanide-doped upconversion nanocrystals. *Chem Soc Rev*. 2009; 38: 976-89.
34. Zhou J, Liu Z, Li FY. Upconversion nanophosphors for small-animal imaging. *Chem Soc Rev*. 2012; 41: 1323-49.
35. Soukka T, Rantanen T, Kuningas K. Photon upconversion in homogeneous fluorescence-based bioanalytical assays. *Fluoresc Methods Appl Spectrosc Imaging Probes*. 2008; 1130: 188-200.
36. Helmchen F, Denk W. Deep tissue two-photon microscopy. *Nat Methods*. 2005; 2: 932-40.
37. Larson DR, Zipfel WR, Williams RM, Clark SW, Bruchez MP, Wise FW, Webb WW. Water-soluble quantum dots for multiphoton fluorescence imaging in vivo. *Science*. 2003; 300: 1434-36.
38. Heike S, Mader, Peter Kele, Sayed M Saleh and Otto S Wolfbeis. Upconverting luminescent nanoparticles for use in bioconjugation and bioimaging. *Curr Opin Chem Biol*. 2010, 14: 582-596.
39. Lu AH, Salabas EL, Schuth F. Magnetic nanoparticles: Synthesis, protection, functionalization, and application. *Angew Chem Int Ed*. 2007; 46: 1222-44.
40. Quan ZW, Wang ZL, Yang PP, Lin J, Fang JY. Synthesis and characterization of high-quality ZnS, ZnS: Mn<sup>2+</sup>, and ZnS: Mn<sup>2+</sup>/ZnS (core/shell) luminescent nanocrystals. *Inorg Chem*. 2007; 46: 1354-60.
41. Quan ZW, Yan DM, Li CX, Kong DY, Yang PP, Cheng ZY, Lin J. Multicolor Tuning of Manganese-Doped ZnS Colloidal Nanocrystals. *Langmuir*. 2009; 25: 10259-62.
42. Tian Q, Tao K, Li WW, Sun K. Hot-Injection Approach for Two-Stage Formed Hexagonal NaYF<sub>4</sub>:Yb, Er Nanocrystals. *J Phys Chem C*. 2011; 115: 22886-892.
43. Zhang YW, Sun X, Si R, You LP, Yan CH. Single-crystalline and monodisperse LaF<sub>3</sub> triangular nanoplates from a single-source precursor. *J Am Chem Soc*. 2005; 127: 3260-61.
44. Li ZQ, Zhang Y. An efficient and user-friendly method for the synthesis of hexagonal-phase NaYF<sub>4</sub>:Yb,Er/Tm nanocrystals with controllable shape and upconversion fluorescence. *Nanotechnology*. 2008; 19: 345606.
45. Chen GY, Ohulchanskyy TY, Kachynski A, Agren H, Prasad PN. Intense Visible and Near-Infrared Upconversion Photoluminescence in Colloidal LiYF<sub>4</sub>:Er<sup>3+</sup> Nanocrystals under Excitation at 1490 nm. *ACS Nano*. 2011; 5: 4981-86.
46. Wang J, Wang F, Wang C, Liu Z, Liu XG. Single-Band Upconversion Emission in Lanthanide-Doped KMnF<sub>3</sub> Nanocrystals. *Angew Chem Int Ed*. 2011; 50: 10369-372.
47. Yang DM, Li CX, Li GQ, Shang MM, Kang XJ, Lin J. Colloidal synthesis and remarkable enhancement of the upconversion luminescence of BaGdF<sub>5</sub>:Yb<sup>3+</sup>/Er<sup>3+</sup> nanoparticles by active-shell modification. *J Mater Chem*. 2011; 21: 5923-27.
48. Zhang H, Li YJ, Lin YC, Huang Y, Duan XF. Composition tuning the upconversion emission in NaYF<sub>4</sub>:Yb/Tm hexaplate nanocrystals. *Nanoscale*. 2011; 3: 963-66.
49. Ye XC, Collins JE, Kang YJ, Chen J, Chen DTN, Yodh AG, Murray CB. Morphologically controlled synthesis of colloidal upconversion nanophosphors and their shape-directed self-assembly. *Proc Natl Acad Sci U S A*. 2010; 107: 22430-35.
50. Naccache R, Vetrone F, Mahalingam V, Cuccia LA, Capobianco JA. Controlled Synthesis and Water Dispersibility of Hexagonal Phase NaGdF<sub>4</sub>:Ho<sup>3+</sup>/Yb<sup>3+</sup> Nanoparticles. *Chem Mater*. 2009; 21: 717-23.
51. Bogdan N, Vetrone F, Roy R, Capobianco JA. Carbohydrate-coated lanthanide-doped upconverting nanoparticles for lectin recognition. *J Mater Chem*. 2010; 20: 7543-50.
52. Mahalingam V, Vetrone F, Naccache R, Speghini A, Capobianco JA. Colloidal Tm<sup>3+</sup>/Yb<sup>3+</sup>-Doped LiYF<sub>4</sub> Nanocrystals: Multiple Luminescence Spanning the UV to NIR Regions via Low-Energy Excitation. *Adv Mater*. 2009; 21: 4025-28.
53. Zhan QQ, Qian J, Liang HJ, Somesfalean G, Wang D, He SL, Zhang ZG, Andersson-Engels S. Using 915 nm Laser Excited Tm<sup>3+</sup>/Er<sup>3+</sup>/Ho<sup>3+</sup>-Doped NaYF<sub>4</sub> Upconversion Nanoparticles for in Vitro and Deeper in Vivo Bioimaging without Overheating Irradiation. *ACS Nano*. 2011; 5: 3744-57.
54. Teng X, Zhu YH, Wei W, Wang SC, Huang JF, Naccache R, Hu WB, Tok AIY, Han Y, Zhang QC, Fan QL, Huang W, Capobianco JA, Huang L. Lanthanide-Doped Na<sub>2</sub>ScF<sub>7</sub> Nanocrystals: Crystal Structure Evolution and Multicolor Tuning. *J Am Chem Soc*. 2012; 134: 8340-43.
55. Chen GY, Qiu HL, Fan RW, Hao SW, Tan S, Yang CH, Han G. Lanthanide-doped ultrasmall yttrium fluoride nanocrystals with enhanced multicolor upconversion photoluminescence. *J Mater Chem*. 2012; 22: 20190-96.
56. Du YP, Zhang YW, Sun LD, Yan CH. Luminescent monodisperse nanocrystals of lanthanide oxyfluorides synthesized from trifluoroacetate precursors in high-boiling solvents. *J Phys Chem C*. 2008; 112: 405-15.
57. Shan JN, Ju YG. A single-step synthesis and the kinetic mechanism for monodisperse and hexagonal-phase NaYF<sub>4</sub>:Yb, Er upconversion nanophosphors. *Nanotechnology*. 2009; 20: 275603.
58. Mai HX, Zhang YW, Sun LD, Yan CH. Size- and phase-controlled synthesis of monodisperse NaYF<sub>4</sub>:Yb,Er nanocrystals from a unique delayed nucleation pathway monitored with upconversion spectroscopy. *J Phys Chem C*. 2007; 111: 13730.
59. Boyer JC, Cuccia LA, Capobianco JA. Synthesis of colloidal upconverting NaYF<sub>4</sub>:Er<sup>3+</sup>/Yb<sup>3+</sup> and Tm<sup>3+</sup>/Yb<sup>3+</sup> monodisperse nanocrystals. *Nano Lett*. 2007; 7: 847-52.
60. Yi G, Sun B, Yang F, Chen D, Zhou Y, Cheng J. Synthesis and characterization of high-efficiency nanocrystal up-conversion phosphors: Ytterbium and erbium codoped lanthanum molybdate. *Chem Mater*. 2002; 14: 2910-14.
61. Fan X, Pi D, Wang F, Qiu J, Wang M. Hydrothermal synthesis and luminescence behavior of lanthanide-doped GdF<sub>3</sub> nanoparticles. *Trans Nanotechnol*. 2006; 5: 123-28.
62. Zhang F, Wan Y, Yu T, Zhang FQ, Shi Y, Xie S, Li S, Li Y, Xu L, Tu B, Zhao D. Uniform nanostructured arrays of sodium rare-earth fluorides for highly efficient multicolor upconversion luminescence. *Angew Chem Int Ed*. 2007; 46: 7976-79.
63. Wang X, Zhuang J, Peng Q, Li YD. A general strategy for nanocrystal synthesis. *Nature*. 2005; 437: 121-124.
64. Li CX, Quan ZW, Yang J, Yang PP, Lin J. Highly uniform and monodisperse beta-NaYF<sub>4</sub>: Ln<sup>3+</sup> (Ln = Eu, Tb, Yb/Er, and Yb/Tm) hexagonal microprism crystals: Hydrothermal synthesis and luminescent properties. *Inorg Chem*. 2007; 46: 6329-37.
65. Su YG, Li LP, Li GS. NaYF<sub>4</sub>:Eu<sup>2+</sup> microcrystals: Synthesis and intense blue luminescence. *Cryst Growth Des*. 2008; 8: 2678-83.
66. Zhuang JL, Liang LF, Sung HY, Yang XF, Wu MM, Williams ID, Feng SH, Su Q. Controlled hydrothermal growth and up-conversion emission of NaLnF<sub>4</sub> (Ln = Y, Dy-Yb). *Inorg Chem*. 2007; 46: 5404-10.
67. Li CX, Yang J, et al. Different microstructures of NaYF<sub>4</sub> fabricated by hydrothermal process: Effects of pH values and fluoride sources. *Chem Mater*. 2007; 19: 4933-42.
68. Wang GF, Qin WP, Wang LL, Wei GD, Zhu PF, Wang DF, Ding FH. Synthesis and upconversion luminescence properties of NaYF<sub>4</sub>:Yb<sup>3+</sup>/Er<sup>3+</sup> microspheres. *J Rare Earths*. 2009; 27: 394-397.
69. Zhang F, Wan Y, Yu T, Zhang FQ, Shi YF, Xie SH, Li YG, Xu L, Tu B, Zhao DY. Uniform nanostructured arrays of sodium rare-earth fluorides for highly efficient multicolor upconversion luminescence. *Angew Chem Int Ed*. 2007; 46: 7976-79.
70. Wang F, Han Y, Lim CS, Lu YH, Wang J, Xu J, Chen HY, Zhang C, Hong MH, Liu XG. Simultaneous phase and size control of upconversion nanocrystals through lanthanide doping. *Nature*. 2010; 463: 1061-65.
71. Zhang F, Li J, Shan J, Xu L, Zhao DY. Shape, Size, and Phase-Controlled Rare-Earth Fluoride Nanocrystals with Optical Up-Conversion Properties. *Chem Eur J*. 2009; 15: 11010-19.
72. Li CX, Zhang CM, Hou ZY, Wang LL, Quan ZW, Lian HZ, Lin J. beta-NaYF<sub>4</sub> and beta-NaYF<sub>4</sub>:Eu<sup>3+</sup> Microstructures: Morphology Control and Tunable Luminescence Properties. *J Phys Chem C*. 2009; 113: 2332-39.
73. Qiu HL, Chen GY, Sun L, Hao SW, Han G, Yang CH. Ethylenediaminetetraacetic acid (EDTA)-controlled synthesis of multicolor lanthanide doped BaYF<sub>5</sub> upconversion nanocrystals. *J Mater Chem*. 2011; 21:17202-208.
74. Hampl J, Hall M, Mufti NA, Yao YM, MacQueen DB, Wright WH, Cooper DE. Upconverting phosphor reporters in immunochromatographic assays. *Anal Biochem*. 2001; 288: 176-87.
75. van de Rijke F, Zijlmans H, Li S, Vail T, Raap AK, Niedala RS, Tanke HJ. Up-converting phosphor reporters for nucleic acid microarrays. *Nat Biotechnol*. 2001; 19: 273-76.
76. Wang YH, Shen P, Li CY, Wang YY, Liu ZH. Upconversion Fluorescence Resonance Energy Transfer Based Biosensor for Ultrasensitive Detection of Matrix Metalloproteinase-2 in Blood. *Anal Chem*. 2012; 84: 1466-73.
77. Wang M, Hou W, Mi CC, Wang WX, Xu ZR, Teng HH, Mao SK. Immunoassay of goat antihuman immunoglobulin G antibody based on luminescence resonance energy transfer between near-infrared respon-

- sive NaYF<sub>4</sub>:Yb, Er upconversion fluorescent nanoparticles and gold nanoparticles. *Anal Chem.* 2009; 81: 8783-89.
78. Kuningas K, Ukonaho T, Pakkila H, Rantanen T, Rosenberg J, Lovgren T, Soukka T. Upconversion fluorescence resonance energy transfer in a homogeneous immunoassay for estradiol. *Anal Chem.* 2006; 78: 4690-96.
  79. Kuningas K, Pakkila H, Ukonaho T, Rantanen T, Lovgren T, Soukka T. Upconversion fluorescence enables homogeneous immunoassay in whole blood. *Clin Chem.* 2007; 53: 145-46.
  80. Saleh SM, Ali R, Hirsch T, Wolfbeis OS. Detection of biotin-avidin affinity binding by exploiting a self-referenced system composed of upconverting luminescent nanoparticles and gold nanoparticles. *J Nanopart Res.* 2011; 13: 4603-11.
  81. Wang LY, Yan RX, Huo ZY, Wang L, Zeng JH, Bao H, Wang X, Peng Q, Li YD. Fluorescence resonant energy transfer biosensor based on upconversion-luminescent nanoparticles. *Angew Chem Int Ed Engl.* 2005; 44: 6054-57.
  82. Liu C, Wang Z, Jia H, Li Z. Efficient fluorescence resonance energy transfer between upconversion nanophosphors and graphene oxide: a highly sensitive biosensing platform. *Chem Commun.* 2011; 47: 4661-63.
  83. Corstjens PLAM, Zuiderwijk M, Nilsson M, Feindt H, Niedbala RS, Tanke HJ. Lateral-flow and up-converting phosphor reporters to detect single-stranded nucleic acids in a sandwich-hybridization assay. *Anal Biochem.* 2003; 312: 191-200.
  84. Zhang P, Rogelj S, Nguyen K, Wheeler D. Design of a highly sensitive and specific nucleotide sensor based on photon upconverting particles. *J Am Chem Soc.* 2006; 128: 12410-11.
  85. Duan N, Wu SJ, Zhu CQ, Ma XY, Wang ZP, Yu Y, Jiang Y. Dual-color upconversion fluorescence and aptamer-functionalized magnetic nanoparticles-based bioassay for the simultaneous detection of Salmonella Typhimurium and Staphylococcus aureus. *Analytica Chimica Acta.* 2012; 723: 1-6.
  86. Cui QH, Shao Y, Ma K, Xu SJ, Wu F, Liu GY. Upconversion emission of fluorescent silver nanoclusters and in situ selective DNA biosensing. *Analyst.* 2012; 137: 2362-66.
  87. Yao LM, Zhou J, Liu J L, Feng W, Li FY. Iridium-Complex-Modified Upconversion Nanophosphors for Effective LRET Detection of Cyanide Anions in Pure Water. *Adv Funct Mater.* 2012; 22: 2667-72.
  88. Liu Q, Peng J, Sun L, Li FH. High-Efficiency Upconversion Luminescent Sensing and Bioimaging of Hg(II) by Chromophoric Ruthenium Complex-Assembled Nanophosphors. *ACS Nano.* 2011; 5: 8040-48.
  89. Yao LM, Zhou J, Liu J L, Feng W, Li FY. Iridium-Complex-Modified Upconversion Nanophosphors for Effective LRET Detection of Cyanide Anions in Pure Water. *Adv Funct Mater.* 2012; 22: 2667-72.
  90. Kumar M, Zhang P. Highly sensitive and selective label-free optical detection of mercuric ions using photon upconverting nanoparticles. *Biosensors and Bioelectronics.* 2010; 25: 2431-35.
  91. Zhou HP, Xu CH, Sun W, Yan CH. Clean and Flexible Modification Strategy for Carboxyl/Aldehyde-Functionalized Upconversion Nanoparticles and Their Optical Applications. *Adv Funct Mater.* 2009; 19: 3892-3900.
  92. Zhang HD, Sun YH, Ye KQ, Zhang P, Wang Y. Oxygen sensing materials based on mesoporous silica MCM-41 and Pt(II)-porphyrin complexes. *J Mater Chem.* 2005; 15: 3181-86.
  93. Borisov SM, Nuss G, Klimant I. Red Light-Excitable Oxygen Sensing Materials Based on Platinum(II) and Palladium(II) Benzoporphyrins. *Anal Chem.* 2008; 80: 9435-42.
  94. Achatz DE, Meier RJ, Fischer LH, Wolfbeis OS. Luminescent Sensing of Oxygen Using a Quenchable Probe and Upconverting Nanoparticles. *Angew Chem Int Ed.* 2011; 50: 260-63.
  95. Liu LN, Li B, Ying J, Wu XD, Zhao HF, Ren XG, Zhu DX, Su ZM. Synthesis and characterization of a new trifunctional magnetic-photoluminescent -oxygen-sensing nanomaterial. *Nanotechnology.* 2008; 19: 495709.
  96. Sun L, Peng H, Stich MIJ, Achatz DE, Wolfbeis OS. pH sensor based on upconverting luminescent lanthanide nanorods. *Chem Commun.* 2009; 33: 5000-5002.
  97. Wolfbeis OS, Weis L, Leiner MJP, Ziegler WE. Fiber-optic fluorosensor for oxygen and carbon dioxide. *Anal Chem.* 1988; 60: 2028-30.
  98. Ertekin K, Klimant I, Neurauter G, Wolfbeis OS. Characterization of a reservoir-type capillary optical microsensor for CO<sub>2</sub> measurements. *Talanta.* 2003; 59: 261-67.
  99. Ali R, Saleh SM, Meier RJ, Azab HA, Elgawad I, Wolfbeis OS. Upconverting Nanoparticle Based Optical Sensor for Carbon Dioxide. *Sens Actuators B Chem.* 2010; 150:126-31.
  100. Fischer LH, Harms GS, Wolfbeis OS. Upconverting Nanoparticles for Nanoscale Thermometry. *Angew Chem Int Ed.* 2011; 50: 4546-51.
  101. Kusama H, Sovers OJ, Yoshioka T. Line Shift Method for Phosphor Temperature Measurements. *J Appl Phys.* 1976; 15: 2349-58.
  102. Messias DN, Vermelho MVD, Gouveia-Neto AS, Aitchison JS. All optical integrated upconversion fluorescence-based point temperature sensing system using Er<sup>3+</sup>-doped silica-on-silicon waveguides. *Rev Sci Instrum.* 2002; 73: 476-79.
  103. Wang X, Kong XG, Yu Y, Sun YJ, Zhang H. Effect of annealing on upconversion luminescence of ZnO:Er<sup>3+</sup> nanocrystals and high thermal sensitivity. *J Phys Chem C.* 2007; 111: 15119-24.
  104. Lei YQ, Song HW, Yang LM, Yu LX, Liu ZX, Pan GH, Bai X, Fan LB. Upconversion luminescence, intensity saturation effect, and thermal effect in Gd<sub>2</sub>O<sub>3</sub>:Er<sup>3+</sup>, Yb<sup>3+</sup> nanowires. *J Chem Phys.* 2005; 123: 174710.
  105. Wang Y, Tu LP, Zhao JW, Sun YJ, Kong XG, Zhang H. Upconversion Luminescence of beta-NaYF<sub>4</sub>:Yb<sup>3+</sup>, Er<sup>3+</sup>@beta-NaYF<sub>4</sub> Core/Shell Nanoparticles: Excitation Power, Density and Surface Dependence. *J Phys Chem C.* 2009; 113: 7164-69.
  106. Bai X, Song HW, Pan GH, Lei YQ, Wang T, Ren XG, Lu SZ, Dong B, Dai QL, Fan L. Size-dependent upconversion luminescence in Er<sup>3+</sup>/Yb<sup>3+</sup>-codoped nanocrystalline yttria: Saturation and thermal effects. *J Phys Chem C.* 2007; 111: 13611-17.
  107. Da Silva CJ, De Araujo MT, Gouveia-Neto AS. Thermal effect on multiphonon-assisted anti-Stokes excited upconversion fluorescence emission in Yb<sup>3+</sup>-sensitized Er<sup>3+</sup>-doped optical fiber. *Appl Phys B.* 2000; 70:185-88.
  108. Dos Santos PV, De Araujo MT, Gouveia-Neto AS, Neto JAM, Sombra ASB. Optical thermometry through infrared excited upconversion fluorescence emission in Er<sup>3+</sup>- and Er<sup>3+</sup>-Yb<sup>3+</sup>-doped chalcogenide glasses. *IEEE J Quantum Electron QE.* 1999; 35: 395-99.
  109. Berthou H, Jorgensen CK. Optical-Fiber temperature sensor based on upconversion-excited fluorescence. *Opt Lett.* 1990; 15: 1100-02.
  110. Suyver JF, Grimm J, Krämer KW, Güdel HU. Highly efficient near-infrared to visible up-conversion process in NaYF<sub>4</sub>: Er<sup>3+</sup>, Yb<sup>3+</sup>. *J Lumin.* 2005; 114: 53-59.
  111. Wu KY, Cui JB, Kong XX, Wang YJ. Temperature dependent upconversion luminescence of Yb/Er codoped NaYF<sub>4</sub> nanocrystals. *J Appl Phys.* 2011; 110: 053510.
  112. Li DY, Wang YX, Zhang XR, Yang K, Liu L, Song YL. Optical temperature sensor through infrared excited blue upconversion emission in Tm<sup>3+</sup>/Yb<sup>3+</sup> codoped Y<sub>2</sub>O<sub>3</sub>. *Opt Commun.* 2012; 285: 1925-28.
  113. Vetrone F, Naccache R, Zamarron A, de la Fuente AJ, Sanz-Rodríguez F, Capobianco JA et al.. Temperature Sensing Using Fluorescent Nanothermometers. *ACS Nano.* 2010; 4: 3254-58.
  114. Sedlmeier A, Achatz DE, Fischer LH, Gorris HH, Wolfbeis OS. Photon upconverting nanoparticles for luminescent sensing of temperature. *Nanoscale.* 2012; 4: 7090-96.
  115. Chen G, Yang C, Prasad PN. Nanophotonics and Nanochemistry: Controlling the Excitation Dynamics for Frequency Up- and Down-Conversion in Lanthanide-Doped Nanoparticles. *Acc Chem Res.* 2013; DOI:10.1021/ar300270y.